Self-Assembly and Ordering of Electrostatically Stabilized Silica Suspensions

R. KESAVAMOORTHY,*† SHALABH TANDON,* S. XU,* S. JAGANNATHAN,* AND SANFORD A. ASHER*,[1]

*Department of Chemistry, University of Pittsburgh, Pennsylvania 15260, and †Materials Science Division, Indira Gandhi Center for Atomic Research, Kalpakkam 603102, India

Received June 17, 1991; accepted January 14, 1992

We use optical attenuation spectral measurements and diffraction measurements to examine the structural evolution of aqueous suspensions of negatively charged colloidal silica particles in thin quartz cells. The ionic strength in the suspension is monotonically decreased in time by ion-exchange resin. At high ionic strengths, two-dimensional hexagonal order nucleates near the surface of the cell walls, while the regions away from the walls show liquid-like order. At lower ionic strengths, regions near the wall show three-dimensional order, while the interior region shows two-dimensional crystalline order. At the lowest ionic strengths, the entire suspension shows three-dimensional crystalline order.

INTRODUCTION

Concentrated colloidal suspensions show colloidal particle ordering which resembles the gas, liquid, glass, and crystalline phases of atomic and molecular systems (1–5). Colloidal silica particles can acquire a net negative charge when dispersed in water due to the ionization of the surface hydroxyl or other functional groups (6). The resultant repulsive interactions (7) between the negatively charged particles depend on the particle surface charge, the particle concentration, the impurity concentration, the temperature, and the medium dielectric constant (8–10). Depending on the extent of the interparticle interactions, these suspensions will self-assemble into gas, liquid, crystal, and glass phases (1–4).

The long-range ordering of these suspensions is also influenced by the walls of the container (11–15). The self-assembly of colloidal crystalline suspensions orients the highest density planes parallel to the walls of the container (the BCC (110) or FCC (111) planes) (16). This phenomenon can be used to orient and form single-crystal colloidal arrays for use as narrow-band optical rejection filters (4, 17). The orientation of colloidal crystalline suspensions is likely to be sensitive to various properties of the container walls; for example, it was recently suggested that the formation of an image charge in the wall is energetically of major importance for orientation of colloidal suspensions (12, 13).

The time evolution of the ordering proceeds by the way of many intermediate steps, as has been recently demonstrated by the Kossel ring pattern analysis by Sogami and Yoshiyama (15). They concluded that ordering of the monodisperse colloidal suspension contained in a quartz cell evolved from two-dimensional (2-D) HCP structure to normal FCC structure (volume fraction, $\phi > 2\%$) or normal BCC structure ($\phi < 2\%$) through many intermediate steps. Clark *et al.* (11) investigated shear-induced melting of colloidal crystals ($\phi \approx 1\%$) and subsequent reordering on removing the shear. They reported that 2-D HCP layer array structure precedes the formation of the ultimate BCC structure.

[1] To whom the correspondence should be addressed.

0021-9797/92 $5.00

The structure, orientation, and lattice parameters of ordered colloidal crystalline suspensions can be determined by laser diffraction (18–20) or Kossel-ring analysis (11, 14–16, 21–23). If the crystal contains numerous defects, the Kossel-rings and diffraction spots may not be sharp enough to characterize the crystal structure. These defects, which often arise during the transition from the liquid to the crystal phase (9, 24–27), may necessitate the use of additional techniques to determine the crystal structure, orientation, and lattice parameters. Optical attenuation spectroscopy has been used to investigate the ordering in colloidal crystals (8, 22, 28). We demonstrate here that angle-dependent optical attenuation spectroscopy can be easily used to characterize crystal structure even for crystals with numerous defects.

We examine the structural evolution of an aqueous suspension of negatively charged silica particles in a thin quartz cell using optical attenuation spectroscopy and diffraction measurements. The regions near the walls of the container appear to be liquid-like, while the regions away from the surface appear gas-like (complete disorder). As the ionic strength of suspension is decreased by the use of ion-exchange resin, 2-D crystalline order develops near the walls, while liquid-like order is observed in regions away from the walls. Upon further deionization, the suspension shows three-dimensional (3-D) crystalline order near the walls, while regions away from the wall show 2-D order. We demonstrate that the structure, orientation, and the lattice parameter of poorly ordered colloidal suspensions can be unambiguously determined using angle resolved optical attenuation spectroscopy in conjunction with laser diffraction.

EXPERIMENTAL

Colloidal silica particles (145–250 nm in diameter) were synthesized using a modified Stöber process (29, 30). Spectroscopic grade ammonium hydroxide (29.2% Mallinckrodt), tetraethyl orthosilicate (Petrarch), and 2-(4-chlorosulfonylphenyl)-ethyltrimethoxysilane (Petrarch) were used as supplied. The concentration of ammonia was determined by titration with standardized HCl solution, using methyl red as the indicator. A typical experimental procedure is: 44.2 ml of water (24.43 M), 15.5 ml of 14.10 M ammonium hydroxide (1.75 M), and 58.0 ml of methanol (11.57 M) are mixed in a clean, dry 250 ml Erlenmeyer flask. The mixture is sonicated using an ultrasonic bath as 7.5 ml of tetraethyl orthosilicate (TEOS, 0.29 M) is added rapidly to the flask. The reaction mixture shows opalescence about a minute after the addition of TEOS, indicating the initiation of the precipitation reaction. The reaction mixture is vigorously stirred for about 12 h yielding a turbid suspension of colloidal silica. To remove excess TEOS, the suspension was washed with methanol at least three times and redispersed in 20 ml of methanol. These silica particles were functionalized using 2-(4-chlorosulfonylphenyl)-ethyltrimethoxysilane (CETS) according to the following procedure. A 20-ml alcoholic solution of CETS (1/20:v/v) is added to the silica suspension and stirred vigorously for ca. 4 h. The resulting suspension was centrifuged, washed with methanol several times, and redispersed in deionized water. The suspension was then dialyzed for at least 3 days against deionized water containing mixed bed ion-exchange resin using 50,000 MWCO Spectra/Por 6 dialysis tubing (Fisher); the water was changed every 24 h. Finally, the suspension was mixed with ion-exchange resin and gently agitated for 48 h using a mechanical shaker.

The particle diameter was determined by quasi-elastic light scattering (QELS, Langley Ford 1096) and by transmission electron microscopy (TEM). The particle size obtained from these two methods agreed to within ±3%; the monodispersity in size was also better than ±3%. We utilized 245-nm and 140-nm particles in the present study. The concentration (n_p) of silica particles was measured by gravimetry (19) by assuming the density of silica to be 2.1 (6).

The laser diffraction measurements were made on suspensions contained in a quartz cell, ($2.5 \times 2.5 \times .01$ cm^3) mounted on a calibrated rotation stage. The incidence angles (in air) were measured relative to the cell surface normal; i.e., the angle of incidence is defined as 0° when the cell plane normal is parallel to the incident beam direction. The angle measurements are accurate to ±0.5°. The angles in the crystal were calculated from the measured angles (in air) using Snell's law. The diffraction angles were measured by rotating the detector about a vertical axis passing through the cell. The diffracted angle was also measured in some cases by placing a screen in the path of the forward diffracted beams (plane of the screen being perpendicular to the transmitted beam) and measuring the distance between the transmitted and diffracted spots on the screen. Laser excitation was obtained using argon-ion and He–Ne lasers.

The optical attenuation spectra were recorded using a Perkin–Elmer Lambda 9 UV/VIS/NIR spectrophotometer. A rotating stage was placed in the sample compartment of the spectrometer and the quartz cell was mounted such that the beam was focused onto the center of the suspension. The cell was rotated about the vertical axis from the normal incidence (0°). The refractive index, n, of the suspension was measured using a temperature controlled Abbé refractometer (Bausch and Lomb).

RESULTS AND DISCUSSION

Structural Evolution of a 245-nm Silica Particle Suspension

The silica suspension ($n_p = 1.67 \times 10^{12}$/cm^3, $n = 1.338$) was introduced into a quartz cell, which contained a reservoir of mixed bed ion-exchange resin. The suspension initially showed iridescence under white light illumination. When illuminated by the 514.5-nm beam of an argon-ion laser at normal incidence, intense forward scattering (a Debye–Scherrer ring) was observed at a small angle (θ_2) centered around the incident beam (Fig. 1a). Speckle fluctuations (ca. 0.5 s) were observed in this broad halo (Fig. 1b).

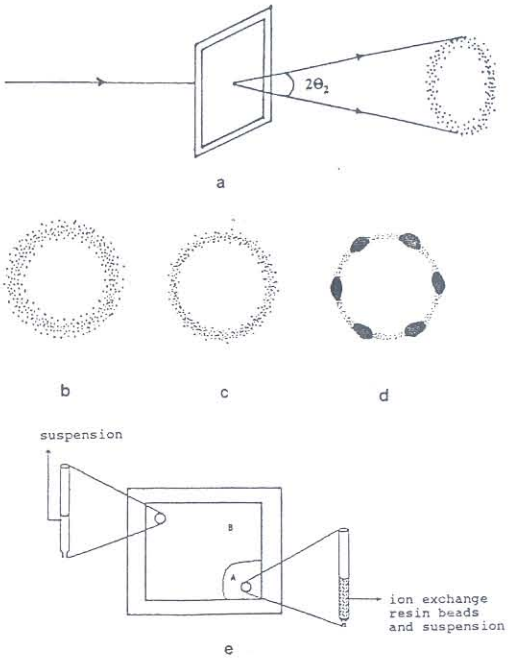

FIG. 1. The scattered intensity pattern of the 245 nm silica particle suspension with $n_p = 1.67 \times 10^{12}$/cm^3, for $\theta_1 = 0°$ and $\lambda = 514.5$ nm. (a) Schematic representation of the optical geometry. (b) One h, (c) 6 h, (d) 2 days after cell preparation. (e) Schematic representation of the cell showing regions A and B.

Debye–Scherrer ring diffraction from colloidal suspensions having liquid-like order is well known (31–33). However, Debye–Scherrer rings (34) are also observed for polycrystalline colloids (19) as well as for a single polycrystalline 2-D colloidal layer (35). A Debye–Scherrer ring should also result from 2-D layers which are stacked one behind the other without any correlation in angle or position of the spheres in one layer relative to another layer. Thus, the broad diffuse ring observed for our suspension could derive from any of these four structures. However, the particle motion in liquid structures will be larger than that in the polycrystalline sample, a polycrystalline 2-D layer, or the 2-D random stacked structures. Speckle fluctuation results from particle movement, and fast fluctuations result from fast particle movement. The ob-

served speckle fluctuation in the broad diffuse ring, which was rapid (periodicity $\approx$ 0.5 s), slowed down, and eventually disappeared after 1 day due to an increased structural ordering. It is likely that the initial broad diffuse ring was produced by liquid-like ordering.

The scattering wavevector, q, is given by

$$q = \frac{4\pi n}{\lambda} \sin\left(\frac{\theta_2^{xtl}}{2}\right), \qquad [1]$$

where θ_2^{xtl} is the diffraction angle in the crystal which is obtained from θ_2 using Snell's law. The diffracted intensity from a liquid-like order is maximum for a value of q which is close to that for the first allowed reciprocal lattice vector present when the liquid freezes into a crystalline order (32). Using the experimentally determined value of q and assuming an FCC structure, we calculate a particle concentration (n_p) of $4.7 \times 10^{12}/cm^3$ ($n_p = 4/a^3$, $a = \sqrt{3}d$, and d is the (111) interplanar spacing). If the liquid crystallized into a BCC lattice, the calculated n_p would be 8% lower. In either case, this calculated particle concentration is threefold larger than that measured by gravimetry ($1.67 \times 10^{12}/cm^3$). This discrepancy in the particle concentration obtained from the two techniques (gravimetry and diffraction) indicates a large inhomogeneity in particle concentration. The region that dominates the diffraction must have the high particle concentration. By conservation of particle number only a small portion of the sample can show this concentration enrichment. Thus, it is likely that the diffraction observed is dominated by a thin (<1 μm) film of liquid-like ordered colloids at the wall (*vide infra*). For example, we can easily observe diffraction from the thin films of ordered colloid which coat the walls of a sample vial containing a crystalline colloid.

Kesavamoorthy *et al.* (12, 13) in a previous study of colloidal polystyrene suspensions using optical microscopy observed an increased particle concentration and an increased particle ordering near the walls of the container compared to the cell interior. They attributed this particle concentration increase to the presence of an attractive potential at the container walls due to image charges induced by the charged colloidal particles on the container walls. The attraction of the colloidal particles by the image charge would result in an increased concentration of the particles adjacent to the walls. Our diffraction measurements indicate that this region of increased particle concentration initially has a liquid-like order. Since a decreased ordering of colloidal suspensions accompanies a particle concentration decrease, we expect that the lowered particle concentration in the cell interior correlates with a nondiffracting gas-like disorder.

As the suspension ionic impurity concentration decreased (due to the presence of ion-exchange resin), the width of the ring decreased (Fig. 1c) and the speckle fluctuation slowed down (ca. 3 s). One day after filling the cell a sixfold pattern of bright spots was observed (superimposed on the diffuse ring). The sixfold pattern was not sharp but was spread over a ca. 10° width along the ring, as shown in Fig. 1d. This pattern did not show speckle fluctuation.

This pattern of spots indicates the existence of 2-D hexagonal arrays (15, 18, 35, 36) which are randomly stacked in the third dimension (e.g., ABCBAC, etc.) (15). This 2-D hexagonal array stacking was previously observed in the structural evolution of colloidal suspensions by Sogami and Yoshiyama (15). We did not observe any diffraction spots which could derive from 3-D crystalline structure (19, 21, 35). The sixfold pattern observed when the incident beam was translated across the cell surface, confirms the existence of 2-D crystalline order along the entire cell surface. Table I lists the measured diffraction angles of the circular rings and the sixfold pattern, as well as the average interparticle separation distance (D) calculated using the 2-D Bragg diffraction equation (18)

$$D = \frac{2\lambda}{\sqrt{3}(\sin\theta_1 + \sin\theta_2)}, \qquad [2]$$

where λ is the incident wavelength, θ_1 is the incidence angle ($\theta_1 = 0°$), and θ_2 is the mea-

sured diffraction angle. Table I also lists the interparticle spacing calculated using Eq. [2] and the gravimetrically determined particle concentration for both FCC and BCC structure.

The value of D (670 nm) obtained from Eq. [2] corresponds to a particle concentration of $4.7 \times 10^{12}/\text{cm}^3$, which is identical to that calculated from the diffuse Debye–Scherrer-type rings. Thus, it appears that the original liquid-like film at the wall has crystallized into a 2-D crystal.

Three days after filling the cell the suspension became inhomogeneous and iridescence of the region close to the ion-exchange reservoir (region A) differed in color from the rest of the cell (region B, Fig. 1e). The interparticle spacing (D) was calculated from the 2-D diffraction patterns (Eq. [2]) to be 948 nm in region A and 812 nm in region B. These values of D (948 nm, 812 nm) are larger than the value 670 nm obtained 1 day after filling the cell. This D-value increase could be due to the increased interparticle repulsive interactions which accompany a reduced ionic impurity concentration, n_i. The interparticle spacing in region A (948 nm) represents the spacing expected for an FCC crystal with the original average particle concentration of $1.67 \times 10^{12}/\text{cm}^3$. This indicates that a similar particle spacing occurs near the wall and in the interior in region A in an ordered structure where 2-D hexagonal layers randomly stack. In region B, the particle concentration calculated from the measured value of D is $2.6 \times 10^{12}/\text{cm}^3$, which is greater than the average particle concentration, but is less than that present when the 2-D crystal just-formed ($4.7 \times 10^{12}/\text{cm}^3$). Thus, in region B the particle concentration near the wall remains higher than that in the interior, but the difference decreases while the ordering increases. The better ordering of region A presumably derives from the lower ionic strength present due to the proximity of region A to the ion-exchange resin reservoir.

The optical attenuation spectra from the two regions (A and B) did not show sharp peaks. Thus, we observe no evidence of 3-D crystalline order. Table I lists the interparticle spacing (D) in the two regions at various times after filling the cell. The "diffraction observed" interparticle spacing initially increases in the period between 6 h and 3 days of filling the sample. This initial increase probably results

TABLE I

The Measured Diffraction Angles from the Suspension of 245-nm Silica Particles ($n_p = 1.67 \times 10^{12}/\text{cm}^3$) and the Calculated Interparticle Separation Distance ($D = 2\lambda/(\sqrt{3}(\sin\theta_2 + \sin\theta_1))$ over a Period of 10 Days ($\lambda = 514.5$ nm and $\theta_1 = 0°$)

Time elapsed (days)	θ_2			D(nm)			Structure
	Homogeneous	Region A	Region B	Homogeneous	Region A	Region B	
1 h	56.2[a]						Liquid-like
6 h	62.4[b]			670			2-D
1	54			734			2-D
3		38.8	47		948	812	2-D
4		41.4	54.4		898	731	2-D
5		58	65.8		700	651	2-D
8	63.5[b]			664			2-D
9	57.4[a]						Liquid-like

Note. 2-D = two-dimensional; D in the (111) plane of a FCC crystal = 946 nm; D in the (110) plane of a BCC crystal = 920 nm.

[a] Fast speckle fluctuation.

[b] Slow speckle fluctuation.

from a decreasing ionic strength, which results in increased interparticle repulsion. In addition, the thickness of the ordered film may increase. After day three the "diffraction observed" interparticle spacing decreases, probably due to an increased impurity concentration due to exhaustion of ion exchange resin.

Structural Characterization of the 140-nm Silica Particle Suspension

A quartz cell filled with a 140-nm silica particle suspension ($n_p = 1.43 \times 10^{13}/cm^3$, $n = 1.339$) showed iridescence under white light illumination and a sixfold diffraction pattern similar to that of Fig. 1d. Figure 2 shows the optical attenuation spectrum of the silica suspension at normal incidence, where a well defined diffraction peak was absent but the attenuation increased rapidly for $\lambda < 510$ nm. For diffraction from a 2-D crystal, with excitation at normal incidence (18)

$$\lambda = \frac{\sqrt{3}}{2} nD \sin \theta_2^{xtl}. \qquad [3]$$

For λ greater than a critical value ($\lambda_c = \sqrt{3}nD/2$), no Bragg diffraction occurs. However, for $\lambda < \lambda_c$, incident light is Bragg diffracted by the 2-D lattice. λ_c is obtained from Fig. 2 by intersecting the straight lines passing through high and low λ regions of the optical attenuation spectrum. λ_c is determined to be 510 nm, which gives a D-value of 439 nm corresponding to a particle concentration of $1.67 \times 10^{13}/cm^3$, slightly higher than the value ($1.43 \times 10^{13}/cm^3$) determined gravimetrically. This result is consistent with the enrichment of the particle concentration for the diffracting parts of the 245-nm particle suspension discussed above. Thus, we conclude that the region nearest to the wall of the 140-nm suspension has an increased particle concentration and is ordered into random stacked 2-D hexagonal layers.

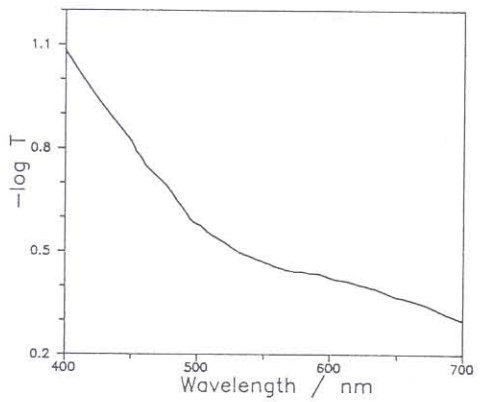

FIG. 2. The optical attenuation spectrum of the 140-nm silica particle suspension ca. 1 h after cell preparation, $n_p = 1.43 \times 10^{13}/cm^3$ and $\theta_1 = 0°$. T is transmittance.

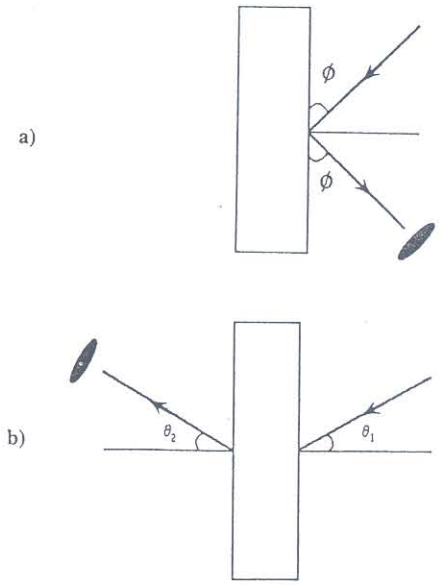

FIG. 3. A schematic representation of the diffraction measurements. (a) Diffraction from a three-dimensional crystal in the reflection geometry. (b) Diffraction from a two-dimensional crystal showing forward diffraction.

After 3 days, diffraction measurements showed a single Bragg diffraction spot spread over a solid angle of ca. 0.04 steradians around the Bragg angle of 71° (ϕ) for 488 nm incident radiation (see Fig. 3a). When the angle of incidence (θ_1) was changed to 42°, a bright, diffuse elliptical spot was seen for forward diffraction (Fig. 3b) at $\theta_2 = 33.5°$ (angles measured in air). Upon translating the cell parallel to its face, θ_2 remained constant but the width of the diffraction spot changed. The intensity

TABLE II

The Measured Angles of Diffraction, ϕ, θ_1, θ_2, in the Suspension of 140-nm Silica Particles with $n_p = 1.43 \times 10^{13}/cm^3$ for Different Wavelengths (λ) and the Calculated Interplanar Separation ($d = (\lambda/2n \sin \phi^{xtl})$) and Interparticle Separation Distance ($D = 2\lambda/(\sqrt{3}(\sin \theta_1 + \sin \theta_2))$

λ	ϕ	θ_1	θ_2	d	D	d/D Experimental
457.9	56	38.5	29.5	376	474	0.8
476.5	63	41	31.5	378	468	0.808
488	71	42	33.5	375.4	462	0.812
514.5	87	44.5	34	384	472	0.813

Note. d/D, expected for FCC = 0.816, for BCC = 0.793.

of the spot decreased slightly as θ_1 was varied away from 42°. Table II lists the angles measured for several excitation wavelengths along with the interparticle spacing (D) calculated using Eq. [2] and the interplanar spacing (d) calculated using (4)

$$d = \frac{m\lambda}{2n \sin \phi^{xtl}}, \qquad [4]$$

where n is the suspension refractive index, ϕ^{xtl} is the Bragg angle for diffraction from a 3-D lattice, and m is the diffraction order. Optical attenuation spectra of this suspension (Figs. 4 and 5; *vide infra*) show peaks corresponding to different sets of planes and indicate the formation of a 3-D crystal structure. The value of D listed in Table II corresponds to a particle concentration of ca. 1.43×10^{13} cm^{-3}, which is the same as that gravimetrically determined. The same particle concentration is calculated from the value of d of Eq. [4]. For the 245-nm spheres above, we observed that the suspension near the wall is more ordered than that in the interior, and the particle concentration in the cell becomes uniform with improved ordering. The present result for the 140-nm silica suspension suggests that 3-D order develops near the wall, while 2-D order exists at the interior after the particle concentration becomes uniform in the cell.

The ion-exchange reservoir was removed from the cell on day 3. On day 6, the sample became inhomogeneous and different regions

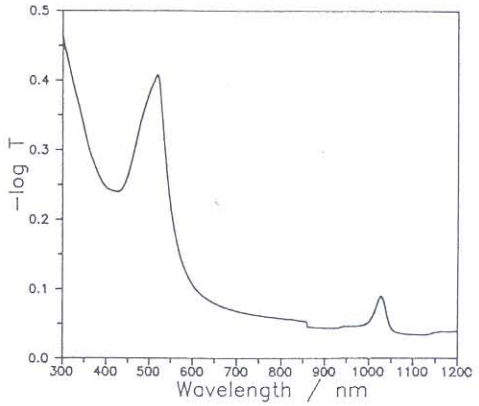

FIG. 4. The optical attenuation spectrum of the 140-nm silica particle suspension with $n_p = 1.43 \times 10^{13}/cm^3$, $\theta_1 = 0°$, 3 days after cell preparation. T is transmittance.

in the suspension showed different iridescence colors under white light illumination. The 3-D Bragg diffraction spot observed in the reflection geometry became very diffuse while the 2-D Bragg spot (in the transmission geometry) became brighter. The intensity of the 2-D Bragg spot decreased slightly upon rotation of the cell around θ_1 ($\theta_1 = 42°$ for the 488-nm beam), but the diffracted spot occurred at an angle satisfying Eq. [2]. The θ_1 intensity dependence on day six is smaller than that for day three. The 2-D diffraction was seen over a wide range of incident angles (17° to 67°). Figure 4 shows the optical attenuation

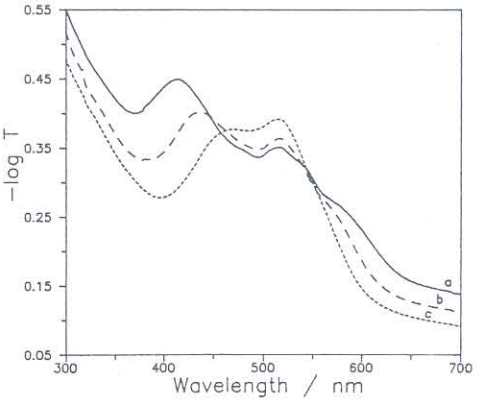

FIG. 5. The optical attenuation spectrum of the 140-nm silica particle suspension with $n_p = 1.43 \times 10^{13}/cm^3$: (a) $\theta_1 = 8°$ (b) $\theta_1 = 6°$, and (c) $\theta_1 = 4°$. T is transmittance.

spectrum of this suspension where the peaks correspond to 3-D Bragg diffraction (*vide infra*). The observed decrease in the ordering on day 6 presumably derives from an increasing n_i due to leaching of ions from the sample cell.

These observations of an increased concentration of 245- and 140-nm silica particles near the wall prior to formation of a 3-D lattice agrees with Kesavamoorthy *et al.* (12, 13), who observed that the particle concentration and the degree of order showed a maximum at the cell container walls. We conclude that an initial 2-D structure with a higher particle concentration nucleates adjacent to the container walls, while the interior regions of the cell remain either gas- or liquid-like. With decreasing n_i the particle concentration difference between the wall vicinity and the interior decreases, the two-dimensionally ordered region near the wall crystallizes into a 3-D FCC crystal while the interior disordered region becomes a 2-D crystal. The appearance of 2-D hexagonal layered structure in the evolution of the colloidal crystal ordering is consistent with other recent investigations (11, 15, 16). The entire suspension crystallizes into a 3-D crystal when the impurity concentration decreases further.

Determination of 3-D Crystal Structure from Angle-Dependent Optical Attenuation Spectra of the 140-nm Silica Particle Suspension

Figures 4 and 5 show the optical attenuation spectra of the 140-nm silica suspension at various incidence angles recorded on day 6. Figure 4 shows a sharp peak at 1051 nm and a broad peak around 525 nm. The ca. 1051 nm attenuation peak shifts to shorter wavelengths and broadens when the incident angle increases from 0° to 10°, while the broad peak at ca. 525 nm becomes better resolved. Since first-order 3-D Bragg diffraction from the planes parallel to the quartz plate gives rise to the longest wavelength peak (1051 nm), the peaks around 525 nm should derive from second-order 3-D Bragg diffraction. The peaks at 525 nm will also have contributions from first-order Bragg diffraction from planes with smaller spacings than those giving rise to the 1051-nm peak. The rapidly decreasing transmittance below 400 nm may derive from diffraction by any coexisting 2-D hexagonal lattice. This suspension shows 3-D diffraction as well as 2-D diffraction as discussed above. We expect that the 3-D crystal exists near the container wall and the 2-D hexagonal layered structure resides in the sample interior.

In order to resolve the diffraction contributions from various planes to the 525-nm peak, we fit the optical attenuation spectra for various incidence angles to a sum of three Gaussian bands and a linear base line. The experimental spectra are shown in Figs. 4 and 5, and Table III lists the best-fit parameters. Obviously, more than three diffraction peaks contribute to the broad 525-nm peak. However, three components allow us to unambiguously establish the dominant structure, orientation and crystal lattice parameter.

The two crystal structures observed in colloidal crystals (body centered cubic, BCC and face centered cubic, FCC) self-assemble such that the highest density planes (BCC (110) or FCC (111)) lie parallel to the container walls. When the FCC (111) or the BCC (110) plane is normal to the incident radiation, the second-order diffraction will overlap with the first-order diffraction wavelengths from the corresponding (200) planes. The angle (β) between two planes in a crystal, (h_1, k_1, l_1) and (h_2, k_2, l_2), is given by (23)

$$\cos\beta = \frac{h_1h_2 + k_1k_2 + l_1l_2}{\sqrt{(h_1^2 + k_1^2 + l_1^2)(h_2^2 + k_2^2 + l_2^2)}}. \quad [5]$$

Using Eqs. [4] and [5], we find that the broad peak centered at ca. 525 nm will have contributions from first-order diffraction of the (002), (020), and (200) planes (λ_{max} = 526 nm), the (220), (202), and (022) planes (λ_{max} = 525 nm), the (311), (131), and (113) planes (λ_{max} = 478 nm), and the (222) planes (λ_{max} = 525.5 nm), as well as from the second-order

TABLE III

Parameters Best Fit to Simulate the Experimental Optical Attenuation Spectra for the 140-nm Silica Particle Suspension for Various Angles of Incidence (θ)

θ	a	b (nm^{-1})	A_1	A_2	A_3	x_1 (nm)	x_2 (nm)	x_3 (nm)	σ_1 (nm)	σ_2 (nm)	σ_3 (nm)
0	.53	700	.19	.095	—	525[a]	480[b]	—	22	22	—
4	.545	673	.183	.135	.044	522	463.5	563	24	27	17.1
5	.601	760	.155	.125	.053	522	453	566	25.5	27.5	18.1
6	.62	763	.135	.118	.05	522	441	573	27	27.5	18.1
7	.654	783	.11	.107	.045	521.5	430	578	27	27	19.9
8	.714	856	.08	.09	.04	521	419.5	583	24	24	22.6
10	.864	1080	.04	.063	.03	520	395	600	22	22	30

Note. The experimental data was best fit to the sum of a linear base line ($y = a - bx$) and three Gaussians with peak heights A_1, A_2, A_3, peak positions x_1, x_2, x_3, and widths σ_1, σ_2, σ_3.

[a] This peak splits into three peaks at x_1, x_2, and x_3 when the incident angle is changed.

[b] This peak for normal incidence derives from the (311) set of planes.

diffraction from the (111) planes (λ_{max} = 525.5 nm) of FCC.

The values of x_2 (nm) found from the fits (Table III) were used to calculate the angles between the putative (200) plane and the incident beam (θ_{200}). The excellent correlation between θ_{200} and the angle of rotation of the sample (Table IV) proves the existence of an FCC structure. We were also able to account for the angular dependence of diffraction from the individual (020) and (002) planes as the cell was rotated. We were able to use the fitted x_2 values to uniquely specify the crystal orientation about the (111) direction. From this crystal orientation we determined the angle between the (020) plane and the incident beam (θ_{020}) and that between (002) plane and the beam (θ_{002}) and we calculated the expected peak positions, λ_3 (Table IV) which agreed well with the experimentally determined x_3 values.

The values of λ_3 calculated assuming a BCC structure are also listed in Table IV, but deviate unacceptably from the experimentally deter-

TABLE IV

The Calculated θ_{200} from the Experimental Peak Positions (x_2) of the Attenuation Spectra of the 140-nm Diameter Silica Particle Suspension with $n_p = 1.43 \times 10^{13}/cm^3$ for Various Angles of Incidence (θ) for FCC and BCC Structures Using the Bragg Law

		FCC			BCC			
θ	x_2 (nm)	θ_{200}	$\theta_{200}=\theta_{002}$	λ_3 (nm)	θ_{200}	θ_{020}	λ_3 (nm)	x_3 (nm)
0	525	35.3	35.3	525	45	45	525	525
4	463.5	30.7	37.4	551.7	38.5	51.5	577	563
5	453	29.9	38	559.6	37.6	52.4	585	566
6	441	29	38.6	567	36.4	53.6	593	573
7	430	28.2	39.2	574.5	35.3	54.7	600	578
8	419.5	27.5	39.8	581	34.4	55.6	608	583
10	395	25.8	41.1	597.2	32.1	57.9	629	600

Note. The calculated θ_{020} and θ_{002} from the geometrical considerations and the corresponding expected Bragg wavelength (λ_3) for various θ for FCC and BCC structures. The experimentally fitted peak positions x_3 compares well with λ_3 for FCC structure.

mined x_3 values. It is also unlikely that x_2 derives from diffraction from the (211) BCC planes (the only other possible diffracting plane in BCC) because of the large differences between λ_3 and x_3.

To obtain further supporting evidence for the FCC structure we determined the ratio of the peak areas at ca. 525 nm and ca. 1051 nm in the attenuation spectrum. The Bragg diffracted intensity from a set of planes in a 3-D crystal, integrated over the wavelength, is given by (37)

$$I_D = I_o Q V, \qquad [6]$$

where I_o is the incident intensity, V is the illuminated crystal volume, and Q is a scattering function defined by (37)

$$Q = \frac{4\pi^4 \alpha^2 n^2 f^2 A}{\lambda^2 v^2}\left(\frac{1 + \cos^2 2\phi^{xtl}}{\sin^2 \phi^{xtl}}\right), \qquad [7]$$

where α is the polarizability of the particle, n is the refractive index of the suspension, v is the volume of the unit cell, λ is the peak position, ϕ^{xtl} is the Bragg angle, A is a constant (4 for BCC and 16 for FCC) (23), and f^2 is the particle structure factor given by

$$f^2 = \left[\frac{3(\sin qa - qa \cos qa)}{q^3 a^3}\right]^2, \qquad [8]$$

where a is the particle radius and q is the scattering vector

$$q = \frac{4\pi n \sin \phi^{xtl}}{\lambda}. \qquad [9]$$

The integrated diffracted intensity which is a function of the peak position λ and the Bragg angle ϕ can be rewritten as

$$I_D = B\left(\frac{1 + \cos^2 2\phi^{xtl}}{\sin^2 \phi^{xtl}}\right)\frac{f^2}{\lambda^2} \qquad [10]$$

where B is a constant.

The attenuation at 1051 and 525 nm is small. Hence, the ratio of integrated diffraction intensities at 1051 and 525 nm for small attenuation is approximately equal to the ratios of the areas of attenuation ($-\log T$) at the respective wavelengths. The ratio of the sum of the first-order integrated diffracted intensities at 525 nm from the (200), (220), (311), and (222) family of planes compared to that for the (111) plane at 1051 nm for an FCC structure is calculated to be 13.7. This agrees extremely well with the experimental value of 14, confirming the initial crystal structure assignment. Table V lists the calculated integrated diffraction intensities for all the relevant planes of an FCC crystal.

A similar calculation carried out for a BCC

TABLE V

The Calculated Three-Dimensional Diffraction Angles (ϕ^{xtl}), the Peak Positions in the Optical Attenuation Spectra, λ, the Particle Structure Factor (f^2), the Diffracted Intensity from Several FCC and BCC Planes and the Calculated Integrated Intensities Along with the Experimental Ratio of Integrated Intensities for the Suspension of 140-nm Silica Particles

Structure	Planes (hkl)	$\phi^{xtl} = 90 - \alpha$	$\lambda = 2nd_{hkl}\sin\phi^{xtl}$	f^2	$I_D/B \times 10^8$ for each set of planes	Ratio of integrated intensities at 525 and 1051 nm: Calculated	Ratio of integrated intensities at 525 and 1051 nm: Experimental
FCC	(111)	90	1051	0.588	1.065		
	(200),(020),(002)	35.3	526	0.328	3.957		
	(220),(202),(022)	54.7	525	0.082	0.4945	13.7	
	(311),(131),(113)	60.5	478	0.044	0.3195		
	(222)	90	525.5	0.037	0.2651		
							14.0
BCC	(110)	90	1051	0.588	1.065		
	(200),(020)	45	526	0.148	1.067	22.2	
	(211),(121)	30	525	0.588	10.646		
	(220)	90	525.5	0.037	0.2651		

crystal gave a too large peak area ratio of 22.2. Table V also lists the diffraction wavelengths that can be expected in the optical attenuation spectrum for normal incidence, from an FCC and a BCC crystal. A comparison of Tables III and V shows that all the expected peaks for an FCC crystal are observed. In contrast, the BCC (310) and (130) planes should show peaks at ca. 420 nm which are not observed.

CONCLUSION

We have studied the time dependence of the crystallization of order within a colloidal silica suspension. We find that the formation of a randomly stacked 2-D crystal is an intermediate stage in the formation of a 3-D crystal. Nucleation occurs at the walls of the container, possibly due to the attraction of image charges. We demonstrate that optical attenuation spectroscopy can be used to unambiguously determine the structure of colloidal suspensions.

REFERENCES

1. Russel, W. B., Saville, D. A., and Schowalter, W. R., "Colloidal Dispersions." Cambridge Univ. Press, New York, 1989.
2. Robbins, M. O., Kremer, K., and Grest, G. S., *J. Chem. Phys.* **88,** 3286 (1988).
3. Kesavamoorthy, R., Sood, A. K., Tata, B. V. R., and Arora, A. K., *J. Phys. C: Solid State Phys.* **21,** 4737 (1988).
4. Asher, S. A., Flaugh, P. L., and Washinger, G., *Appl. Spectrosc.* **1,** 26 (1986).
5. Hone, D., Alexander, S., Chaikin, P. M., and Pincus, P., *J. Chem. Phys.* **79,** 1474 (1983).
6. Iler, R. K., "The Chemistry of Silica," Chap. 3. Wiley, New York, 1979.
7. Verwey, E. J. W., and Overbeek, J. Th. G., "Theory of the Stability of Lyophobic Colloids." Elsevier, Amsterdam, 1948.
8. Okubo, T., *J. Chem. Soc., Faraday Trans. 1* **82,** 3185 (1986).
9. Kesavamoorthy, R., Tata, B. V. R., Arora, A. K., and Sood, A. K., *Phys. Lett. A* **130,** 208 (1989).
10. Grüner, F., and Lehmann, W. P., *J. Phys. A: Math. Gen.* **15,** 2847, (1982).
11. Clark, N. A., Hurd, A. J., and Ackerson, B. J., *Nature* **281,** 57 (1979).
12. Kesavamoorthy, R., Rajalakshmi, M., and Babu Rao, C., *J. Phys: Condens. Matter* **1,** 7149 (1989).
13. Kesavamoorthy, R., Babu Rao, C., and Tata, B. V. R., *J. Phys: Condens. Matter,* in press.
14. Pieranski, P., *Contemp. Phys.* **24,** 25 (1983).
15. Sogami, I. S., and Yoshiyama, T., *Phase Transitions* **21,** 171 (1990).
16. Monovoukas, Y., and Gast, A. P., *J. Colloid Interface Sci.* **128,** 533, (1989).
17. Asher, S. A., U.S. Patents 4,627,689 and 4,632,517.
18. Krieger, I. M., and O'Neill, F. M., *J. Am. Chem. Soc.* **90,** 3114, (1968).
19. Udo, M. K., and de Souza, M. F., *Solid State Commun.* **35,** 907, (1980).
20. Hiltner, P. A., and Krieger, I. M., *J. Chem. Phys.* **73,** 2386 (1969).
21. Rundquist, P. A., Photinos, P., Jagannathan, S., and Asher, S. A., *J. Chem. Phys.* **91,** 4932, (1989).
22. Rundquist, P. A., Jagannathan, S., Kesavamoorthy, R., Brnardic, C., Xu, S., and Asher, S. A., *J. Chem. Phys.* **94,** 711 (1991).
23. Carlson, R. J., and Asher, S. A., *Appl. Spectrosc.* **38,** 297, (1984).
24. Hachisu, S., Kobayashi, Y., and Kose, A., *J. Colloid Interface Sci.* **46,** 470 (1973).
25. Fujita, H., and Amitani, K., *Jpn. J. Appl. Phys.* **16,** 1091 (1977).
26. Ackerson, B. J., and Clark, N. A., *Phys. Rev. Lett.* **46,** 123 (1981).
27. Schaefer, D. W., and Ackerson, B. J., *Phys. Rev. Lett.* **35,** 1448 (1975).
28. Okubo, T., *J. Chem. Soc. Faraday Trans. 1* **84,** 1171 (1988).
29. Stöber, W., Fink, A., and Bohn, E., *J. Colloid Interface Sci.* **26,** 62 (1968).
30. Van Helden, A. K., Jansen, J. W., and Vrij, A., *J. Colloid Interface Sci.* **81,** 354 (1981).
31. Härtl, W., and Versmold, H., *J. Chem. Phys.* **80,** 1387, (1984).
32. Arora, A. K., and Kesavamoorthy, R., *Solid State Commun.* **54,** 1047 (1985).
33. Hurd, A. J., "The Lattice Dynamics of Colloidal Crystals." PhD. Dissertation, University of Colorado, 1981.
34. Warren, B. E., "X-ray Diffraction." Addison–Wesley, Massachusetts, 1969.
35. Ackerson, B. J., and Chowdhury, A. H., *Faraday Discuss. Chem. Soc.* **83,** 309 (1987).
36. Tomita, A., Takano, K., and van de Ven, T. G. M., *J. Colloid Interface Sci.* **81,** 354 (1981).
37. Zachariasen, W. H., "Theory of X-ray Diffraction in Crystals," Chap. 3. Wiley, New York, 1945.